Journal of Structural Chemistry. Vol. 56, No. 3, pp. 557-565, 2015.

AN XPS AND TPD STUDY OF GOLD OXIDE FILMS OBTAINED BY EXPOSURE TO RF-ACTIVATED OXYGEN

A. I. Stadnichenko[1,2], S. V. Koshcheev[1], and A. I. Boronin[1,2]

UDC 544.023.2:544.022.3:542.493:544.72:546.55

Low-temperature oxidation of the polycrystalline surface of bulk metallic gold with radio-frequency activated oxygen is used to obtain oxide films, which are investigated by a combination of X-ray photoelectron spectroscopy (XPS) and temperature programmed desorption (TPD). The XPS estimate for the composition and thickness of the oxide films is close to Au_2O_3 and is 6-10 nm. The analysis of the Au4*f* and O1*s* lines reveals only one state of the oxidized gold, which is described by E_b(Au4*f*) = 85.5 eV, and two nonequivalent states of oxygen with E_b(O1*s*) = 529.3 eV and 530.3 eV, which are uniformly distributed over the oxide film and may be attributed to nonequivalent oxygen states in the gold oxide structure. The thermal stability study shows that the gold oxide decomposes in one stage into metal at a temperature of T_{des} = 530 K. According to the TPD data, the desorption activation energy is E_{des} = 140 kJ/mol. The high-temperature oxidation of the gold surface reveals the formation of dissolved oxygen in bulk gold. This oxygen is characterized by a broad TPD peak with a maximum at T_{des} = 800 K. This oxygen state is not detected by XPS. The concentration of dissolved oxygen is supposed to be below the XPS sensitivity threshold and is estimated at about 1% or less.

DOI: 10.1134/S0022476615030245

Keywords: gold oxide, adsorbed oxygen, gold, surface, XPS, TPD, plasma, oxide film.

INTRODUCTION

Group 11 metals (Cu, Ag) are broadly used as catalysts in many partial and complete oxidation reactions [1, 2]. Previously, it was believed that gold did not have this activity [3]. This was disproved by Haruta *et al.,* who showed a high catalytic activity of nanodisperse gold [1, 4], and the subsequent boom in research literature on gold-containing catalysts [5-7].

The majority of studies are focused on systems containing gold nanoparticles applied on variable-valence oxides (TiO_2, Fe_2O_3, CeO_2, etc.), which are active in oxidative reactions such the CO oxidation reaction [1, 5, 6, 8], propylene epoxidation [9, 10], and other oxidative processes [11-13]. The unique activity of gold catalysts is closely related to the formation of adsorbed oxygen species on the surface of gold nanoparticles, which is broadly discussed in the literature. There are studies suggesting that oxygen is localized at the interface of gold and the support [14, 15] and in quasi-carbonate

[1]Boreskov Institute of Catalysis, Siberian Branch, Russian Academy of Sciences, Novosibirsk, Russia; stad@catalysis.ru. [2]Novosibirsk National Research University, Novosibirsk, Russia. Translated from *Zhurnal Strukturnoi Khimii*, Vol. 56, No. 3, pp. 591-600, May-June, 2015. Original article submitted February 4, 2015.

complexes [16, 17] or hydroxo groups [18] on gold or in the composition of sorbed species on $Au^{\delta+}$ [19]. Under the conditions of oxidation reactions, gold nanoparticles might also oxidize completely, passing into the state of nanooxides [20].

In this context, there is a growing interest in the experimental and theoretical studies on the structure and nature of oxygen bonding with the surface of gold both in nanoparticles and in bulk. It is virtually impossible to obtain XPS data on the state of adsorbed oxygen on the surface of gold nanoparticles due to the low Au concentration in the particles and the overlap with the intense oxygen line from the oxide supports. The alternative way, which is associated with studying adsorbed oxygen on the pure bulk gold surface (foil, single crystals, or powders), encounters a major obstacle, namely, the difficulties of obtaining oxygen species on bulk gold due to the high energy barrier of O_2 adsorption [21, 22].

Different authors proposed different techniques to treat the surface of gold and obtain chemosorbed oxygen on gold: ozone [23, 24], NO_2 [25], and atomic oxygen [26, 27] exposure, oxygen adsorption at high pressures and temperatures [28], etc. Other authors propose more effective approaches in terms of the degree of surface oxidation: electrochemical oxidation of a gold electrode [29], laser ablation [30], magnetron sputtering [31] in an oxygen atmosphere, and microwave [32, 33] or radio-frequency [34, 35] activated oxygen exposure. In the case of electrochemical oxidation, it is difficult to eliminate anion impurities (Cl^-, SO_4^{2-}, etc.) and use the XPS method, which is associated with an electrochemical cell, while microwave or radio-frequency activation may be used in electron spectrometer chambers without any substantial difficulties.

Data on the thermal stability of gold oxides are given in a number of literature sources; however, most of them are focused on physadsorbed oxygen [36, 37] and oxygen in the composition of surface oxides [26, 38] or individual nanoparticles of gold oxides [39].

Thus, the aim of this work is to use a combination of XPS and TPD to investigate oxide layers on the surface of bulk gold, which were obtained at room or higher temperatures using plasma exposure.

EXPERIMENTAL

The experiments were carried out using a VG ESCALAB HP photoelectron spectrometer (VG Scienta, United Kingdom). The residual pressure of background gases in the experiment did not exceed 1×10^{-9} mbar. Photoelectrons were excited with a nonmonochromated primary radiation source (AlK_α line of $h\nu$ = 1486.6 eV). The power dissipation of X-rays in the experiments was 200 W. No sample reduction due to exposure to an X-ray beam was observed. The spectrometer was calibrated by the Au4*f* line with E_b = 84.0 eV and the Cu2$p_{3/2}$ line with E_b = 932.7 eV [40]. The XPS spectra were recorded in a constant transmission energy mode ($h\nu$) of the analyzer. The survey spectra were recorded at $h\nu$ = 100 eV. The precision spectra of the Au4*f*, O1*s*, and C1*s* lines were recorded at $h\nu$ = 20 eV with an energy step of 0.1 eV. In this case, the full width at half maximum for the standard Au4$f_{7/2}$ line was 1.3 eV. To process the data and analyze the spectra, we used the XPS CALC software, which was previously tested on a number of systems [41-43], and the standard graphic packages. The decomposition into components was performed by approximating the peaks with a sum the Lorentzian and Gaussian functions after subtracting the Shirley background. The error of the background subtraction and decomposition procedures did not exceed 1%.

The thermal stability of gol oxide films was investigated by the TPD method using a Q7B quadruple mass spectrometer (Vacuum Generators) mounted in the analyzer chamber in close proximity to the sample surface. In all the TPD experiments, 18, 32, 28, and 44 masses were controlled simultaneously. The experiments also used XPS in a spectrokinetic mode (dynamic photoelectron spectroscopy (D-XPS)). In this case, intensities were recorded at a maximum of the peaks (Au4f_{met}, Au4f_{ox}, and O1*s*) as a function of time during sample heating with normalization by the background line.

Gold was oxidized in a pure oxygen atmosphere (P = 25 Pa) in a radio-frequency plasma (RF-discharge) in the spectrometer preparation chamber. The radio-frequency activation of O_2 was performed at temperatures of 300 K, 507 K, and 527 K, an amplitude of the exciting radiation of 600 W, and a frequency of 12.6 MHz. The sample holder was grounded. The time of the plasma exposure ranged from 0.1 to 20 min.

Polycrystalline gold foil with a purity of 99.99% and a width of 200 μn (EZ OTsM, Verkhnyaya Pyshma, Russia) was used as samples. The surface of the samples was purified by successive cycles of argon-ion etching and annealing at 1023 K. The purity of the gases used in the experiments was controlled with the mass spectrometer. At all the stages of the experiments, no impurities were found on the surface of the samples within the sensitivity of the XPS method. Samples with sizes of 8×23 mm were fixed in a holder with gold wire by spot welding. The holder of special design enabled controlled heating of the samples to a temperature of 1100 K with an accuracy of 0.1 K. The samples were heated with electric current transmitted through them; the temperature was measured with a Pt–Pt/Rh thermocouple welded to the back side of the samples.

RESULTS AND DISCUSSION

The experiments showed that the RF-activated oxygen exposure of the surface of gold foil leads to effective surface oxidation already at room temperature. The use of RF-activated oxygen enables full oxidation of gold to a greater depth of about 10 nm. Fig. 1 shows the spectra of the core levels of Au4*f* and O1*s* with the decomposition into individual components obtained by oxidizing the gold surface for 1-30-240 s.

The decomposition of the Au4*f* spectra into individual components (Fig. 1*a*) shows that there are two distinct states of gold: metallic gold (E_b = 84.0 eV) and gold in the composition of the oxide (E_b = 85.6 eV). During the plasma exposure, the peak with E_b = 85.6 eV begins to prevail, suggesting intense multilayer oxidation of bulk gold. With increasing time of the RF-discharge exposure, the halfwidth of the oxide line is observed to decrease from 1.75 eV to 1.52 eV, which may indicate the structuring and ordering of the oxide layer because poorly structured nanosystems and applied particles with a multidisperse size distribution are characterized by an increase in the width of the photoelectron lines.

With increasing oxidation, there is a gradual shift in the position of the line of oxidized gold toward high binding energies (Fig. 1*a*). Starting from the minimum degree of oxidation (RF discharge for 1 s) to the maximum oxidation (RF discharge for 4-5 min), the line of gold oxide Au4f_{ox} shifts by 0.3 eV. It is unlikely that this shift is related to the change in the degree of gold oxidation because gold is known to have only one stable oxidized state, namely, Au^{3+} [29]; moreover, a change in the degree of oxidation in metals usually leads to much larger shifts in the core lines.

It should be noted that even a 10-min or longer exposure to RF-activated oxygen does not result in a complete disappearance of the metallic component (E_b(Au4*f*) = 84.0 eV) from the Au4*f* spectra. This effect was also observed by other authors during intense oxidation of a gold surface [30, 32].

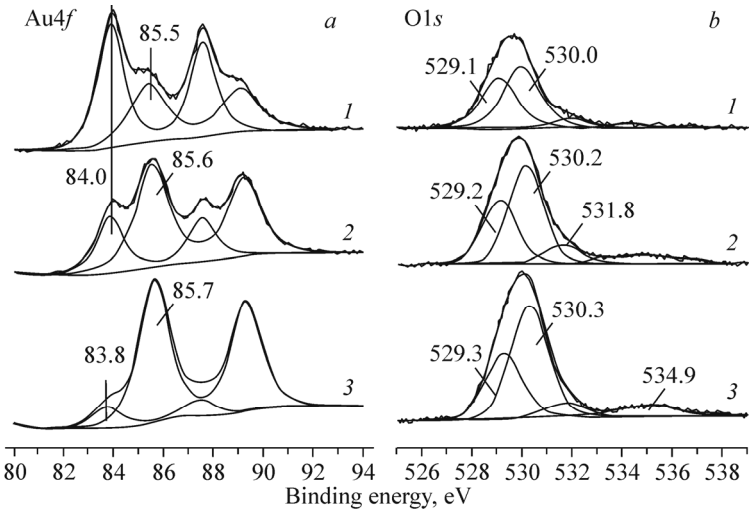

Fig. 1. Decomposition of the Au4*f* (*a*) and O1*s* (*b*) spectra into components of oxide films obtained by the oxidation of gold foil in an oxygen atmosphere $P(O_2)$ = 25 Pa, T = 300 K using RF-discharge for 1 s (curve *1*), 30 s (curve *2*), and 240 s (curve *3*).

The Au^0 state that is constantly observed in the spectra can be directly explained by the fact that the width of the oxide layer is less than the depth of XPS analysis. Another suggestion is that the observed presence of metallic gold on the oxide film surface is due to small metallic clusters that may form on the surface because of the decomposition of the oxide film under X-rays. This instability of gold oxide under X-rays was observed by many authors [32, 44]. Another reason for the appearance of metal on the oxide surface might be the reduction of gold by reacting with the spectrometer background gases (CO and H_2). The suggestion about the formation of small metal clusters on the oxide surface is confirmed by the shift of the metallic component of Au4*f* toward smaller energies to E_b = 83.6 eV, which is typical of fine gold [45].

However, the most likely explanation for the existence of the metallic component in the Au4*f* spectra even under the most intense oxidation is the occlusion of a metallic core inside the oxide film shell. This suggestion is based on the observed constancy of this metallic state in the spectra when the surface is oxidized using an RF discharge. Moreover, the data of angular photoemission experiments show that the metal is distributed over the entire oxide layer, suggesting that the small metal inclusions are located inside the oxide film. In this case, the size of the metallic cores is at a minimum because the observed shift of the metallic component toward smaller binding energies to $E_b(Au4f_{7/2})$ = 83.6 eV means that the sample passes from the bulk state to cluster forms, which are characterized by greater localization of electrons due to a sharp increase in the share of surface atoms in the cluster [46].

The amount of oxygen obtained on the surface of bulk gold using an RF discharge is in all cases much higher than the monolayer coatings. At the same time, the full width of the oxygen peak at half maximum (FWHM) is over 2 eV. This means that the observed oxygen peak has a complex structure and consists of several components. Fig. 1*b* shows the O1*s* spectra and their decomposition into individual components after a microwave exposure of 1 s (curve *1*), 30 s (*2*), and 4 min (*3*). The integral peak of O1*s* decomposes into four components: α_1 with E_b = 529.1 eV, α_2 with E_b = 530.0 eV, α_3 with E_b = 531.8 eV, and α_4 with E_b = 534.3-535.5 eV. The first two components, α_1 and α_2, are attributed to oxygen in the composition of the three-dimensional gold oxide Au_2O_3, whose structure contains oxygen atoms with a nonequivalent location [47, 48]. The increase in the time of surface oxidation leads to a gradual shift of the α_1 and α_2 components toward higher binding energies. In the literature, these shifts are associated with the dielectric properties of the grown films [30].

Specially designed angular-resolved XPS experiments reliably confirmed the absence of a concentration gradient along the depth of the oxide layer for all the oxygen species. This means that all the four oxygen species are evenly distributed in the XPS analysis zone, which is defined by electrons' mean free path (mfp, λ). The calculated concentration also showed that, except at the very beginning of the oxidation, the ratio between the α_1 and α_2 oxygen species is constant: α_1:α_2 = 1:1.6. Thus, we can conclude that an oxide film consisting of oxide nanoparticles is formed on the surface. This explains the presence of the α_1 species throughout the depth of the oxide layer and the constancy of the α_1 to α_2 ratio. The formation of similar films of nanostructured oxides were recorded earlier during the oxidation of copper foil [49]. Based on the areas of the corresponding components, we can calculate the average size of the oxide nanoparticles. If we assume that the particles have a spherical shape, the calculated size of one particle is ~30-40 Å in diameter. If we assume the formation of layered structures consisting of oxide flakes, the thickness of a flake is ~13-16 Å given that its linear size is not known.

The oxygen species α_3 with E_b = 532.0±0.2 eV has a fairly high binding energy. This species is observed to form during oxygen exposures of any length. Some authors attribute this binding energy on the surface of gold to oxygen in the composition of OH-groups or water [29, 32]. The value of E_b = 532.1 eV indicates that there is a chemical bond between the oxygen atoms; i.e., these might be peroxide-type species, which are stable at room temperature. Similar conclusions about the nature of oxygen with a similar binding energy were made in [30] for the formation of oxygen on a gold surface by laser deposition.

Long-time exposures to microwave activated oxygen lead not only to effective oxidation of the surface of gold but also to the appearance of a fundamentally new oxygen state (the species α_4) in the system. This species has an anomalously high binding energy E_b = 534.5-535.5 eV; adsorbed oxygen species with such a high binding energy E_b(O1*s*) are not known in literature. It turns out that the state α_4 is an integral description of a range of species in the composition of the gold oxide. The decomposition of the spectra showed that there are two high-energy components with E_b of 534.6 eV and 535.7 eV. It

should be noted that these components do not appear during the initial phases of gold oxidation; they are observed only at maximum degrees of surface oxidation; therefore, α_4 can be assumed to appear owing to the formation of a thick film of the three-dimensional gold oxide. There are several hypotheses to explain the chemical nature of these α_4 species:

First, the growth of the oxide film is due to the diffusion of gold atoms toward the surface; therefore, the oxide might have occluded oxygen molecules in the voids formed because the species with E_b = 535.8 eV is close in binding energy to oxygen in the gaseous phase, whose binding energy is E_b(O1*s*) = 538.0 eV. (This value was also determined using a VG ESCALAB High Pressure spectrometer and takes into account the work function of the material analyzer.) In this case, a part of oxygen molecules may be located in nanopores with gold oxide walls. The state of oxygen molecules inside these nanopores is likely to be similar to the physadsorbed state. However, even such a weak interaction of O_2 molecules with the nanopore walls can reduce the binding energy by 1-1.5 eV, compared with gaseous O_2 in the free state (the species with E_b = 535.7 eV) due to the change in extraatomic relaxation [40, 50].

According to the second hypothesis, this oxygen state may be attributed to oxygen in the composition of superoxide groups localized on the oxide surface. In [51], these superoxide groups are reported to form on a nickel surface with binding energies of E_b(O1*s*) = 536-537 eV. Finally, it cannot be ruled out that the origin of the high-energy peaks is associated with photoionization due to elastic electron losses (*electron shake-up*) and the appearance of shake-up satellites in the spectra. This approach does not rule out that the satellite lines in the range 534-537 eV are attributed to molecular oxygen in the system (the species α_2) and the appearance of a shake-up satellite in the O1*s* spectra is explained by the electronic structure of the occupied and vacant orbitals of the O–O bond.

The thermal stability of the oxygen species was assessed by temperature programmed desorption (TPD). At the same time, we recorded the intensities of the oxygen peak (*m*/*e* = 32) in the mass spectrum and those of photoelectron lines in the D-XPS mode (Au4f_{met} – E_b = 84.0 eV, Au4f_{ox} – E_b = 85.5 eV, O1*s* – E_b = 530.0 eV and the background line – E_b = 508.0 eV) (Fig. 2*a*). The D-XPS curves were normalized by the background lines and differentiated to determine the temperature of the main intensity changes more accurately (Fig. 2*b*). As is evident from the D-XPS data, the decomposition of the gold oxide (Au_{ox} 85.5 eV) and increase in the amount of metallic gold (Au_{met} 84.0 eV) coincides with oxygen desorption from the surface (E_b(O1*s*) = 530.0 eV). The release of O_2 in the TPD spectra was reported at the same temperature. It is also evident from the spectrokinetic curves that the Au_2O_3 oxide decomposes in one stage without the formation of any intermediate compounds. Thus, the gold oxide Au_2O_3 (E_b(Au4$f_{7/2}$) = 85.5 eV and E_b(O1*s*) = 530.0 eV) is stable at temperatures below 500 K and decomposes at *T* = 530 K.

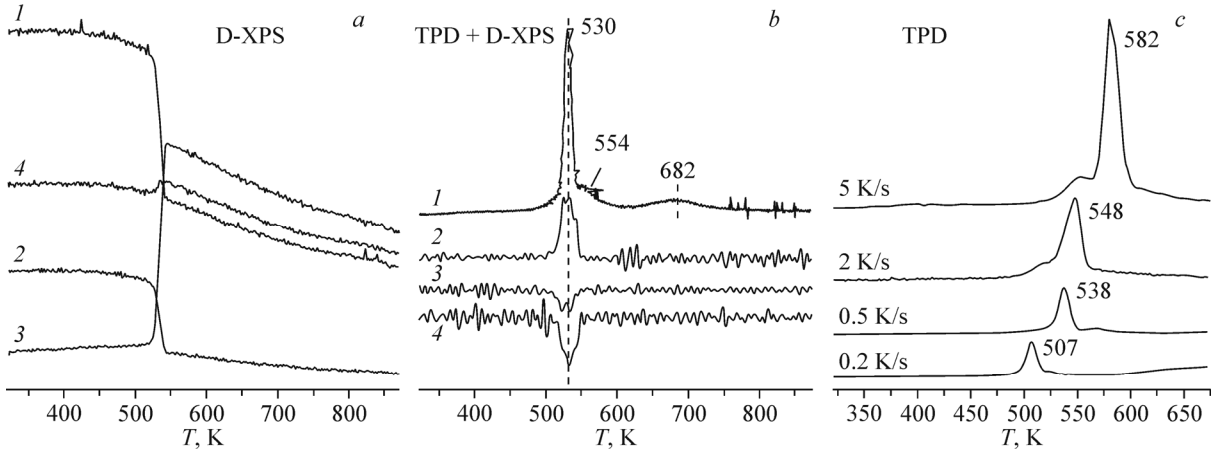

Fig. 2. D-XPS curves of the intensity peaks O1*s* = 530.0 эВ (curve *1*), Au4f_{ox} = 85.5 eV (curve *2*), Au4f_{met} = 84.0 eV (curve *3*), and background line = 508.0 eV (curve *4*) (*a*); TPD: mass-spectrum of oxygen *m*/*e* = 32 (*1*) and differentiated D-XPS curves of metallic gold E_b (Au4*f*) == 84.0 eV (*2*), oxidized gold E_b (Au4*f*) = 85.5 eV (*3*), and oxygen E_b (O1*s*) = 530.0 eV (*4*) (*b*); TPD spectra of oxygen *m*/*e* = 32 from the surface of bulk gold after an exposure to RF-activated oxygen in the gaseous phase (P_{O_2} = 25 Pa, *T* = 300 K, τ = 2 min) (*c*). The heating rates are 5 K/s, 2 K/s, 0.5 K/s, and 0.2 K/s.

The TPD spectra have two more temperature-desorption oxygen peaks, which are not reflected in the D-XPS curves (Fig. 2*b*, curve *1*). While the peak with T_{max} = 554 K can be attributed to oxygen desorption in the oxide film formed by a mixture of two- and three-dimensional oxides, the peak with T_{max} = 682 K is most likely related to the interim formation of ″subsurface″ oxygen, which is broadly discussed in the literature for various metals [52, 53]. It should be noted that a similar desorption temperature of T = 654 K was reported by Madix [26] and Gottfried *et al.* [54] when applying the ion-implantation technique for the formation of adsorbed oxygen on the surface of gold. The high-temperature state of oxygen adsorbed on a gold surface is manifest in the case of restructuring, mass transfer or deep oxidation of oxygen implantation down into many layers, which indicates that the subsequent thermal regeneration of the loosened gold surface may be accompanied by the occlusion of a part of oxygen atoms and molecules and small clusters of two- and three-dimensional oxides.

Moreover, beginning from T = 380 K, the TPD spectra show (Fig. 3*b*, curve *1a*) a slight increase in oxygen pressure, which is not manifest as a peak. This increase is well described by the assumption about the slow desorption of weakly bound oxygen species from the surface of the oxide film. The fact that the plateau in the TPD spectra does not disappear and extends from 380 to 500 K is evidence of the ongoing desorption from the surface, which means that this species is replenished by oxygen diffusion from other species and this diffusion is likely to be a limiting factor.

The TPD experiments were carried out at different heating rates (Fig. 2*c*). The increase in the heating rate leads to an increase in the intensity of the TPD peak and its shift toward higher temperatures (Fig. 2*c*). Thus, TPD experiments at minimum heating rates yield the most accurate data on the actual thermal stability of the adsorption layer. It should be noted that thermal stability studies reported in the literature were carried out at higher heating rates: 8.5 K/s by Koel [38] and 21.5 K/s by Madix [26].

Heating-rate variation can be used to calculate the value of E_d:

$$\ln(T_p^2/\beta) = E_d/R * 1/T_p + \ln(E_d/\nu_1 R),$$

where T_p is the absolute temperature of the TPD peak, K; β is the heating rate, K; and R is the universal gas constant.

Plotting the dependence of $\ln(T_p^2/\beta)$ on $1/T_p$ helps determine the desorption activation energy E_d from the line slope:

$$\mathrm{tg}(\alpha) = 12125.499 = E_{des}/R, \text{ whence } E_{des} \approx 101 \text{ kJ/mol}.$$

This value of desorption activation energy appears to be reasonable and close to those obtained by other authors: 140 kJ/mol by Gottfried [55] and 162 kJ/mol by Madix [26]. Nevertheless, one should admit that the desorption activation energy value calculated by heating-rate variation may differ from the actual one because oxygen desorption from the adsorption oxygen layer obtained by an RF-discharge is not an elementary process but includes, in addition to a purely

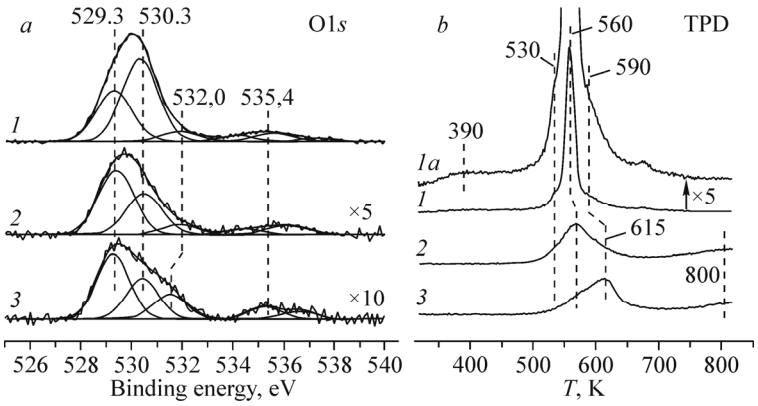

Fig. 3. O1*s* spectra and their decomposition (*a*) and TPD spectra of oxygen (*b*) from the surface of bulk gold after an exposure to microwave activated oxygen in the gaseous phase (P_{O_2} = 25 Pa, τ = 10 min) at temperatures of T 300 (*1*), 503 (*2*, the O1*s* spectrum is magnified by a factor of 5), 523 K (*3*, the O1*s* spectrum is magnified by a factor of 10).

chemical stage of atomic oxygen recombination, the stages of phase transitions, in particular, the likely transition of the three-dimensional oxide into the two-dimensional one.

In the case of RF activation of oxygen in the gaseous phase, surface oxidation is effective already at room temperatures. RF-activated oxygen exposures at sample temperatures close to that of decomposition of the gold oxide Au_2O_3 allow one to avoid the formation of thick oxide films on the surface (Fig. 3). However, even at a temperature of 523 K, one can observe the appearance of small amounts of oxide, which is evidenced by a low-intensity peak with E_b = 85.8 eV in the Au4*f* spectra. A comparison of the O1*s* spectra obtained after exposures at high temperatures and at room temperature (Fig. 3*a*) shows that the increase in temperature leads to the disappearance of the high-energy oxygen species α_4 ($E_{св}$(O1*s*) ~ 535 eV). In the O1*s* spectra obtained after a high-temperature plasma exposure, this component was included into the decomposition procedure; however, it should be noted that the actual intensity of the peaks attributed to the α_4 species is rather low. It is possible that the components α_4 in the decomposition reflect the changes in the shape of the background or noise manifestations.

The increase in the sample temperature during the interaction with oxygen plasma leads to a visible decrease in the intensity of the O1*s* signal from adsorbed oxygen species. Here noteworthy is the visible change in the shape and position of the TPD curves (Fig. 3*b*). There are no narrow peaks indicating the decomposition of the two- or three-dimensional oxide, but there is a shift in the maximum of the TPD peak toward higher temperatures (Fig. 3*b*, *3*). These TPD data are compelling evidence that, at increased temperatures of plasma exposure, not oxides but other, more stable oxygen species form on the polycrystalline foil. However, a comparison of the O1*s* spectra given in Fig. 3*a* shows that the position of the components α_1-O (E_b(O1*s*) = 529.3 eV) and α_2-O (E_b(O1*s*) = 530.3 eV) of the oxygen species does not change and does not depend on the plasma exposure temperature; there is only a change in their relative quantities. Considering these data as a whole, we can assume that the nature of these high-temperature oxygen species is associated with their subsurface localization as a result of surface restructuring during the formation and decomposition of gold oxides. The observed high-temperature oxygen species are, in fact, the subsurface-localized remnants of oxide particles occluded with a metal film formed during a rapid decomposition of the oxide film.

These conclusions on the localization of oxide nanoclusters inside the subsurface region of gold are confirmed by the TPD data given in Fig. 3*b*. Evidently, when the surface is exposed to RF-activated oxygen at high temperatures, the TPD spectra show a smooth increase in oxygen desorption from the surface at temperatures above 770 K. The absence of a pronounced maximum and the fact that the release of oxygen continues for some time when the heating is over suggests that the system contains diffusion (dissolved in bulk metal) oxygen. The formation of the diffusion (dissolved) oxygen in bulk gold can be explained by the formation and decomposition of gold oxide particles.

The high-temperature O_2 plasma exposures lead both to the formation and immediate decomposition of the gold oxide whereby a part of oxide nanoclusters are fixed inside the metallic film of gold. In this case there are good conditions for oxygen release both into the gaseous phase and bulk metal during the heating of the sample. As regards the diffusion oxygen, it is not reflected in the XPS spectra, which means that it is dissolved deep inside the bulk of the metallic foil.

CONCLUSIONS

This study showed that an RF-activated oxygen exposure of the surface of gold foil leads to effective surface oxidation. By changing the surface exposure time, we showed that there is a possibility of varying the thickness of the oxide film. The data obtained suggest that the chosen surface exposure method for polycrystalline gold leads to a comparatively rapid growth of the oxide film with the formation of predominantly three-dimensional Au_2O_3 particles. Based on the analysis of the Au4*f* spectra obtained after long RF-discharge exposures, we calculated the thickness of the resulting oxide film. Depending on the experiment conditions, the oxide film has a thickness of 10 Å to 60 Å. The XPS analysis of the oxide film composition found only one state of oxidized gold: Au^{3+} with E_b(Au4*f*) = 85.5 eV and two ground states of oxygen: α_1-O (E_b(O1*s*) = 529.1 eV) and α_2-O (E_b(O1*s*) = 530.0 eV). The thermal stability study of the resulting oxide films showed that

they decompose in one stage into metal at a temperature of T_{des} = 530 K. The oxygen desorption activation energy was estimated by heating-rate variation to be E_{des} = 101 kJ/mol. The plasma oxidation of the surface of gold at high temperatures stimulates the formation of oxide species of gold, which are occluded in the subsurface layers of polycrystalline gold, which leads to an apparent increase in thermal stability to 610 K. The study detected the formation of oxygen dissolved in the bulk of the gold foil; the dissolved oxygen is characterized by a broad desorption peak at around T_{des} = 800 K.

The work was partially supported by the Program of the President of the Russian Federation for young scientists and postgraduates (SP-2585.2015.1).

REFERENCES

1. M. Haruta and M. Daté, *Appl. Catal., A*, **222,** 427-437 (2001).
2. F. Boccuzzi, A. Chiorino, M. Manzoli, D. Andreeva, T. Tabakova, L. Ilieva, and V. Iadakiev, *Catal. Today*, **75,** 169-175 (2002).
3. B. Hammer and J. K. Norskov, *Nature*, **376,** 238-240 (1995).
4. M. Haruta, N. Yamada, T. Kobayashi, and S. Iijima, *J. Catal*., **115,** 301 (1989).
5. S. K. Hashmi and G. J. Hutchings, *Angew. Chem. Int. Ed*., **45,** 7896-7936 (2006).
6. R. Meyer, C. Lemire, S. K. Shaikhutdinov, and H.-J. Freund, *Gold Bull*., **37,** 72-124 (2004).
7. G. C. Bond and D. T. Thompson, *Catal. Rev. Sci. Eng*., **41,** 319-388 (1999).
8. H. Lian, M. Jia, W. Pan, Y. Li, W. Zhang, and D. Jiang, *Catal. Commun*., **6,** 47-51 (2005).
9. T. Hayashi, K. Tanaka, and M. Haruta, *J. Catal*., **575,** 566-575 (1998).
10. Y. Ryabenkova, Q. He, P. J. Miedziak, N. F. Dummer, S. H. Taylor, A. F. Carley, et al., *Catal. Today*, **203,** 139-145 (2013).
11. D. Andreeva, R. Nedialkova, L. Ilieva, and V. Abrashev, *Appl. Catal. A*, **246,** 29-38 (2003).
12. L. Ilieva, G. Pantaleo, I. Ivanov, R. Zanella, J. W. Sobczak, W. Lisowski, et al., *Catal. Today*, **175,** 411-419 (2011).
13. M. Turner, O. P. H. Vaughan, and R. M. Lambert, *Chem. Commun. (Cambrige, U. K.)*, 2316-2318 (2008).
14. M. M. Schubert, S. Hackenberg, A. C. van Veen, M. Muhler, V. Plzak, and R. J. Behm, *J. Catal*., **197,** 113-122 (2001).
15. M. Okumura, J. M. Coronado, J. Soria, M. Haruta, and J. C. Conesa, *J. Catal*., **203,** 168-174 (2001).
16. C. H. Kim and L. T. Thompson, *J. Catal*., **230,** 66-74 (2005).
17. M. M. Schubert, A. Venugopal, M. J. Kahlich, V. Plzak, and R. J. Behm, *J. Catal*., **222,** 32-40 (2004).
18. M. A. Debeila, R. P. K. Wells, and J. A. Anderson, *J. Catal*., **239,** 162-172 (2006).
19. S. Minico, S. Scire, C. Crisafulli, A. M. Visco, and S. Galvagno, *Catal. Lett*., **47,** 273-276 (1997).
20. D. C. Lim, I. Lopez-Salido, R. Dietsche, M. Bubek, and Y. D. Kim, *Surf. Sci*., **600,** 507-513 (2006).
21. Z.-P. Liu, P. Hu, and A. Alavi, *J. Am. Chem. Soc*., **124,** 14770-14779 (2002).
22. W. T. Wallace, R. B. Wyrwas, R. Whetten, R. Mitric, and V. Bonačić-Koutecky, *J. Am. Chem. Soc*., **125,** 8408-8414 (2003).
23. A. Y. Klyushin, T. C. R. Rocha, M. Hävecker, A. Knop-Gericke, and R. Schlögl, *Phys. Chem. Chem. Phys*., **16,** 7881-7896 (2014).
24. J. Kim, E. Samano, and B. E. Koel, *Surf. Sci*., **600,** 4622-4632 (2006).
25. D. T. Wickham, B. A. Banse, and B. E. Koel, *Catal. Lett*., **6,** 163-172 (1990).
26. N. D. S. Canning, D. Outka, and R. J. Madix, *Surf. Sci*., **141,** 240 (1984).
27. C. Linsmeier and J. Wanner, *Surf. Sci*., **305,** 454-456 (2000).
28. J. Chevrier, L. Huang, P. Zeppenfeld, and G. Comsa, *Surf. Sci*., **355,** 1-12 (1996).
29. K. Juodkazias, J. Juodkazyte, V. Jasulaitiene, A. Lukinskas, and B. Sebeka, *Electrochem. Commun*., **2**, No. 7, 503-507 (2000).
30. E. Irissou, M. C. Denis, M. Chaker, and D. Guay, *Thin Solid Films*, **472,** 49-57 (2005).

31. V. Matolín, M. Cabala, I. Matolínová, M. Škoda, J. Libra, M. Václavů, et al., *J. Phys. D: Appl. Phys*., **42,** 115301-115308 (2009).
32. B. Koslowski, H.-G. Boyen, C. Wilderotter, G. Kastle, P. Ziemann, R. Wahrenburg, and P. Oelhafen, *Surf. Sci*., **475,** 1-10 (2001).
33. S. M. McClure, T. S. Kim, J. D. Stiehl, P. L. Tanaka, and C. B. Mullins, *J. Phys. Chem. B*, **108,** 17952-17958 (2004).
34. P. Fuchs, *Appl. Surf. Sci*., **256,** 1382-1390 (2009).
35. A. I. Stadnichenko, S. V. Koshcheev, and A. I. Boronin, *Moscow Univ. Chem. Bull*., **62,** 343-349 (2007).
36. J. Kim, Z. Dohnalek, and B. D. Kay, *J. Am. Chem. Soc*., **127,** 14592/14593 (2005).
37. J. M. Gottfried, K. J. Schmidt, S. L. M. Schroeder, and K. Christmann, *Surf. Sci*., **525,** 184-196 (2003).
38. N. Saliba, D. H. Parker, and B. E. Koel, *Surf. Sci*., **410,** 270-282 (1998).
39. D. C. Lim, I. Lopez-Salido, R. Dietsche, M. Bubek, and Y. D. Kim, *Surf. Sci*., **600,** 507-513 (2006).
40. D. Briggs and M. P. Seah (eds.), *Surface Analysis by Auger and X-Ray Photoelectron Spectroscopy*, 2nd ed., Wiley, Chichester (1990).
41. D. A. Svintsitskiy, A. I. Stadnichenko, D. V. Demidov, S. V. Koscheev, and A. I. Boronin, *Appl. Surf. Sci*., **257,** 8542-8549 (2011).
42. L. S. Kibis, A. I. Stadnichenko, S. V. Koscheev, V. I. Zaikovskii, and A. I. Boronin, *J. Phys. Chem. C*, **116,** No. 36, 19342-19348 (2012).
43. O. Yu. Podyacheva, A. I. Stadnichenko, S. A. Yashnik, O. A. Stonkus, E. M. Slavinskaya, A. I. Boronin, A. V. Puzynin, and Z. R. Ismagilov, *Chin. J. Catal*., **35,** 960-969 (2014).
44. H. Tsai, E. Hu, K. Perng, M. Chen, J.-C. Wu, and Y.-S. Chang, *Surf. Sci. Lett*., **537,** L447-L450 (2003).
45. W. F. Egelhoff, *Surf. Sci. Rep*., **6,** 253-415 (1987).
46. R. van Hardeveld and F. Hartog, *Surf. Sci*., **15,** 189-230 (1969).
47. B. Y. P. G. Jones, H. Rumpel, E. Schwarzmann, and G. M. Sheldrick, *Acta Crystallogr. Sect. B*, **35,** 1435-1437 (1979).
48. H. Shi, R. Asahi, and C. Stampfl, *Phys. Rev. B*, **75**, 205125-205133 (2007).
49. A. I. Stadnichenko, A. M. Sorokin, and A. I. Boronin, *J. Struct. Chem.,* **49**, No. 2, 341-347 (2008).
50. P. H. Citrin, G. K. Wertheim, and Y. Baer, *Phys. Rev. Lett*., **41,** 1425 (1978).
51. C. M. Kim, H. S. Jeong, and E. H. Kim, *Surf. Sci*., **459**, Nos. 1/2, L457-L461 (2000).
52. A. I. Titkov, A. N. Salanov, S. V. Koscheev, and A. I. Boronin, *React. Kinet. Catal. Lett*., **86**, No. 2, 371-379 (2005).
53. N. Mcmillan, T. Lele, C. Snively, and J. Lauterbach, *Catal. Today*, **105,** 244-253 (2005).
54. J. M. Gottfried, N. Elghobashi, S. L. M. Schroeder, and K. Christmann, *Surf. Sci*., **523,** 89-102 (2003).
55. J. M. Gottfried, K. J. Schmidt, S. L. M. Schroeder, and K. Christmann, *Surf. Sci*., **525,** 184-196 (2003).